Atmospheric
Chemistry
and Physics

Open Access

Mass spectrometry of refractory black carbon particles from six sources: carbon-cluster and oxygenated ions

J. C. Corbin[1], B. Sierau[1], M. Gysel[2], M. Laborde[2,*], A. Keller[3], J. Kim[4], A. Petzold[4,**], T. B. Onasch[5,6], U. Lohmann[1], and A. A. Mensah[1]

[1]ETH Zurich, Institute for Atmospheric and Climate Science, Zurich, Switzerland
[2]Paul Scherrer Institute, Laboratory of Atmospheric Chemistry, 5232 Villigen PSI, Switzerland
[3]Institute of Aerosol and Sensor Technology, University of Applied Sciences Northwestern Switzerland, Windisch, Switzerland
[4]Deutsches Zentrum für Luft- und Raumfahrt, Institut für Physik der Atmosphäre, 82234 Oberpfaffenhofen, Germany
[5]Aerodyne Research Inc., Billerica, Massachusetts, USA
[6]Boston College, Chestnut Hill, Massachusetts, USA
*now at: Aerosol Consulting ML GmbH, Ennetbaden, Switzerland, & Ecotech Pty Ltd., Australia
**now at: Institut für Energie- und Klimaforschung IEK-8: Troposphäre, Forschungszentrum Jülich GmbH, 52425 Jülich, Germany

Correspondence to: J. C. Corbin (joel.corbin@env.ethz.ch)

Abstract. We discuss the major mass spectral features of different types of refractory carbonaceous particles, ionized after laser vaporization with an Aerodyne high-resolution soot-particle aerosol mass spectrometer (SP-AMS). The SP-AMS was operated with a switchable 1064 nm laser and a 600 °C thermal vaporizer, yielding respective measurements of the refractory and non-refractory particle components. Six samples were investigated, all of which were composed primarily of refractory material: fuel-rich and fuel-lean propane/air diffusion-flame combustion particles; graphite-spark-generated particles; a commercial fullerene-enriched soot; Regal Black, a commercial carbon black; and nascent aircraft-turbine combustion particles.

All samples exhibited a spectrum of carbon-cluster ions C_x^{n+} in their refractory mass spectrum. Smaller clusters ($x < 6$) were found to dominate the C_x^{n+} distribution. For fullerene soot, fuel-rich-flame particles and spark-generated particles, significant C_x^{n+} clusters at $x \gg 6$ were present, with significant contributions from multiply charged ions ($n > 1$). In all six cases, the ions C_1^+ and C_3^+ contributed over 60 % to the total $C_{1<x<16}^+$ intensity. Furthermore, the ratio of these major ions C_1^+/C_3^+ could be used to predict whether significant C_x^{n+} signals with $x > 5$ were present. When such signals were present, C_1^+/C_3^+ was close to 1. When absent, C_1^+/C_3^+ was < 0.8. This ratio may therefore serve as a proxy to distinguish between the two types of spectra in atmospheric SP-AMS measurements.

Significant refractory oxygenated ions such as CO^+ and CO_2^+ were also observed for all samples. We discuss these signals in detail for Regal Black, and describe their formation via decomposition of oxygenated moieties incorporated into the refractory carbon structure. These species may be of importance in atmospheric processes such as water uptake and heterogeneous chemistry.

If atmospherically stable, these oxidized species may be useful for distinguishing between different combustion sources. If unstable, they may provide a means to estimate the atmospheric age of an rBC sample. Future studies should attempt to establish which of these scenarios is more realistic.

1 Introduction

Combustion-generated particles represent the most efficient light-absorbing particles in the atmosphere. In addition to affecting the radiative balance of the earth, such particles may also enhance glacial melting (Flanner et al., 2007), alter

convection and precipitation (Ramanathan and Carmichael, 2008), react with atmospheric trace gases (Monge et al., 2010), and serve as cloud condensation (Hitzenberger et al., 2003; Tritscher et al., 2011; Engelhart et al., 2012; Martin et al., 2012) and possibly ice nuclei (DeMott et al., 1999; Koehler et al., 2009; Corbin et al., 2012). Consideration of the short atmospheric lifetime (days to weeks, Cape et al., 2012), human health effects, and damage to crops associated with combustion-generated particles has led to their being highlighted as ideal candidates for near-term climate mitigation (Shindell et al., 2012; Bond et al., 2013).

While the light-absorbing component of combustion particles is a major anthropogenic climate-warming agent, its warming effect can be counteracted by light-scattering from internally mixed, non-absorbing material (IPCC, 2007; Ramanathan and Carmichael, 2008; Bond et al., 2013). Depending on the combustion, significant amounts of such material may be emitted at the source (Bond et al., 2013). Co-emitted reactive gases may be oxidized in the atmosphere to form less volatile compounds, which condense onto absorbing particles and significantly increase their non-absorbing fraction over time (Cappa et al., 2013). This so-called secondary material is frequently hygroscopic, affecting particle cloud droplet activation and thus lifetime, in addition to radiative properties (Bond et al., 2013). Yet secondary material, in particular particulate secondary organic matter (SOM), is not well represented by most climate models (Bond et al., 2013). Thus, quantification of the composition and evolution of the light-absorbing and the non-absorbing components of combustion particles is a current topic of major interest (Cappa et al., 2012, 2013; Jacobson, 2013).

The need for an improved representation of the mixing of light-absorbing particles with secondary material motivates the atmospheric source apportionment of aged, combustion-generated particles. Techniques to measure and apportion combustion emissions to their sources include radiocarbon measurements (e.g., Zencak et al., 2007); X-ray, Raman or electron spectroscopy (Robertson, 2002); the combination of elemental carbon measurements with other tracers (e.g., Jeong et al., 2013); measurements of light-absorption Ångström exponents (e.g., Sandradewi et al., 2008); and single-particle mass spectrometry (e.g., Toner et al., 2008). The first three of these methods require offline filter analysis and do not provide high-time-resolution information. High-time-resolution measurements of light-absorbing carbonaceous particles are made by a number of mass- or light-absorption-based instruments (e.g., Petzold and Schönlinner, 2004; Laborde et al., 2012), but mass spectrometry stands out for its ability to characterize chemical differences between combustion particles. Such chemical characterization may provide information on particle source, mixing state (Liu et al., 2013), and chemical evolution.

Commercial aerosol mass spectrometers typically employ either thermal-desorption or laser desorption/ionization (LDI) vaporizers. Thermal-desorption vaporization does not detect the refractory, light-absorbing carbon of combustion particles. On the other hand, LDI mass spectrometers may detect both refractory and non-refractory components. These mass spectrometers are often capable of detecting individual particles, which might thereafter be attributed to specific sources, such as different vehicle types (Toner et al., 2008). Multiple studies have correlated single-particle LDI signals with collocated mass measurements in order to estimate chemically resolved mass loadings (Pratt and Prather, 2012; Healy et al., 2013). However, the sensitivity of LDI to matrix-influenced charge-transfer reactions (Reilly et al., 2000) and to the particle-to-particle variability of reactions within the ablation plume (Reinard and Johnston, 2008) hinders a robust quantification of atmospheric aerosols.

Although not able to directly measure refractory carbon species, the Aerodyne aerosol mass spectrometer (AMS) (Jayne et al., 2000; Canagaratna et al., 2007) has in recent years been pivotal in quantifying source contributions to organic aerosol loadings (Zhang et al., 2011). The AMS quantifies non-refractory particulate matter (NR-PM) by thermal-desorption vaporization at 600 °C, followed by a separate electron-impact ionization step. This two-step vaporization–ionization process yields especially reproducible mass spectra, facilitating mass quantification (Jimenez et al., 2003). Yet the AMS does not vaporize refractory particulate matter (R-PM) such as that in dust, sea salt, or refractory black carbon particles (rBC).

A modified AMS, the soot-particle AMS (SP-AMS), addresses this limitation with the addition of a 1064 nm laser vaporizer (Onasch et al., 2012). Whereas the AMS vaporizes only NR-PM, the SP-AMS vaporizes 1064 nm light-absorbing refractory particulate matter (LR-PM) via radiative heating. LR-PM includes rBC as a subset. During radiative heating of LR-PM, any less-refractory PM internally mixed with LR-PM may be vaporized by conduction. This commonly includes such species as sulfates, nitrates, and organic matter. These conductively vaporized species distinguish the SP-AMS from incandescence-based techniques such as the single-particle soot photometer (SP2), which quantify rBC mass based only on the refractory particulate component that is heated to rBC vaporization temperature. The relationship between these PM subsets is further illustrated in the Supplement (Sect. S1).

This paper presents a discussion of the SP-AMS mass spectra of six types of rBC particles. The six samples comprise five laboratory aerosols as well as emissions from an aircraft engine within a test cell at the Zurich Airport in Switzerland. The discussion emphasizes refractory mass spectral features relevant to the interpretation of ambient SP-AMS measurements. First, signals from carbon-cluster ions were considered. Two ratios between the most common such ions were identified, and were directly related to the overall carbon-cluster ion distribution. For an atmospheric aerosol containing a variety of rBC types, this result may be useful in apportioning the SP-AMS carbon-cluster signals between

sources. Second, oxygenated-carbon ions originating from the rBC were identified and attributed to refractory oxygenated moieties within the rBC. The potential atmospheric impacts of these ions are discussed.

2 Experimental

2.1 Laboratory setup

A series of laboratory experiments were performed in January 2012 as part of an intensive laboratory campaign, "BC-Act". This campaign was undertaken at ETH Zurich to investigate the physical, chemical and optical properties of various rBC particle types using a range of techniques.

The laboratory setup is shown in Fig. 1. rBC particles were generated by various methods (Sect. 2.3), diluted when necessary, and introduced into a chamber with a residence time of approximately 30 min. Oil-free stainless-steel tubing was used prior to the SP-AMS. All gases used were of high purity (grade 5.6 synthetic air, grade 6.0 nitrogen, grade 6.0 argon). Dilution was achieved using either an ejector diluter (VKL10, PALAS GmbH, Germany) with synthetic air or a filter system. The filter system split samples between two short parallel sections of tubing, one of which contained both a filter and a valve; the valve was used to control the degree of sample filtration. From the residence chamber, particles were passed through two bipolar chargers, split into two equal sample flows, and size-selected by a differential mobility analyzer (DMA) in each line before characterization by a suite of instruments. This suite included a single-particle soot photometer (SP2) and aerosol particle mass analyzer (APM), which measure incandescent rBC mass and shape-independent single-particle mass, respectively. These SP2 and APM data were used as a reference for the non-refractory mass contained in the different rBC particle types (Sect. S7). A previous publication has discussed selected single-particle soot photometer (SP2) results from this study (Gysel et al., 2012); the present work focusses on results obtained with the SP-AMS.

The two DMAs (DMA 1: custom-built (Winklmayr et al., 1991; Wiedensohler et al., 2012); DMA 2: TSI model 3071, TSI Inc., Minnesota, USA) were each calibrated using polystyrene latex spheres of the diameters used in the experiments. The calibration particles were 125 nm (Duke Scientific Corp., Palo Alto, USA), 200 nm (Duke Corp.) and 305 nm (BS-Partikel GmbH, Wiesbaden, Germany) in diameter. Some experiments were also performed with 500 nm-selected particles and polydisperse aerosols. The sample flow rate through each DMA was consistent at $2\,L\,min^{-1}$, with a $5\,L\,min^{-1}$ sheath flow. The DMA resolution – the ratio of the maximum to the full-width-half-maximum of the predicted DMA transfer function – was therefore 2.5. This is lower than the manufacturer-recommended resolution of 10, and was chosen to maximize the particulate mass loading
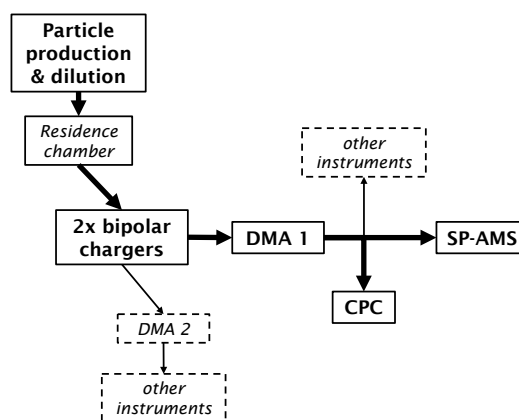

Fig. 1. Laboratory setup used for all samples except turbine particles. Aerosols were diluted before passing through a $1\,m^3$ residence chamber with residence time $\sim 30\,min$. Particles then flowed through two bipolar chargers at $4\,L\,min^{-1}$ before being split equally between two DMAs.

downstream of the DMA. This setting gives a broad-enough transfer function that a minor overlap would have occurred between different size-selected experiments (Table 1). A condensation particle counter (CPC, model 3010, TSI Inc. USA) monitored particle number concentrations during each experiment.

2.2 Soot-Particle Aerosol Mass Spectrometer

The Aerodyne soot-particle aerosol mass spectrometer (SP-AMS) is an evolution of the Aerodyne high-resolution time-of-flight aerosol mass spectrometer (AMS), to include a continuous-wave 1064 nm laser vaporizer. In this section we describe the operation principles of the standard AMS, followed by a description of the SP-AMS and its sampling configuration.

The AMS (Aerodyne Research Inc., Massachusetts, USA) has been described in detail by Jayne et al. (2000) and Canagaratna et al. (2007). Briefly, aerosols are sampled through an aerodynamic lens to focus particles before they enter a vacuum chamber. Upon entering the chamber, particles are accelerated to their size-dependent terminal velocity and traverse a sizing region before reaching the vaporizer. The AMS vaporizer is a porous-tungsten inverted cone held at $\sim$ 600 °C, which flash-vaporizes non-refractory aerosol components before 70 eV electron-impact ionization (EI) and high-resolution time-of-flight mass analysis. Interference by gases and internal background signals is accounted for by regularly blocking incoming particles with a mechanical disc, as well as periodically filtering the sampled aerosol. In an alternate mode of operation, the mechanical disc is continuously rotated, and positioned such that particles are pulsed through a mechanical slit on its edge. This so-called particle time-of-flight (PToF) mode allows measurements to be taken

Table 1. Summary of samples, sizes measured, and experimental programme.

Aerosol	Abbreviation	Mobility Diameter [nm]	Date
CAST Black	CBK	125, 200, 305	Jan 26
CAST Brown	CBW	125, 200, 305	Jan 27
Spark-generated particles	GFG	125, 200, 305, 500	Jan 30
Regal Black	RB	125, 200, 305, 500	Jan 31
Fullerene-Enriched Soot	FS	125, 200, 305, 500	Feb 1
Thermodenuded CBW	CBWTD	125, 200, 305	Feb 2
Aircraft gas-turbine particles	TU	Polydisperse (mode 25)	Apr 30

as a function of particle vacuum aerodynamic diameter at the cost of signal-to-noise; the chopper has a duty cycle of only 1 %. We refer to "MS mode" to distinguish normal measurements from PToF measurements.

The SP-AMS (Onasch et al., 2012) is identical to the AMS but for the addition of a switchable, active-cavity, continuous-wave 1064 nm Nd:YAG laser (Droplet Measurement Technologies, CO, USA). The laser is similar to that used by the SP2 (Schwarz et al., 2006; Laborde et al., 2012) but has higher fluence. The laser is installed orthogonally to both the particle beam and ion extraction path, intersecting the EI ionization chamber. Whereas the AMS detects only NR-PM, the SP-AMS vaporizes LR-PM by radiative heating (notably rBC and metals) as well as PM associated with LR-PM by conductive heating, as described in the introduction. After vaporization, EI ionization and mass analysis proceed in a similar fashion to the AMS. The different modes of vaporization in the AMS and SP-AMS may result in differences between the internal energies of the resulting vapors, which may influence consequent EI fragmentation patterns (Alfarra, 2004; Onasch et al., 2012).

In this study, the AMS and SP-AMS vaporizers were employed simultaneously, such that particles transited through the laser beam on their way to the AMS vaporizer. Laser-absorbing particles such as rBC particles are therefore expected to vaporize within the laser beam, without reaching the AMS vaporizer (Onasch et al., 2012). The SP-AMS laser was switched on and off during sampling, to obtain both "regular" AMS mass spectra (laser off) and SP-AMS mass spectra (laser on). The AMS vaporizer was always on. The ion time-of-flight chamber was operated in the shorter of two flight modes (V-mode), utilizing a single pass through the reflectron. PToF mode was employed 25 % of the time for all laboratory samples and measurements were averaged over 90 s. Data were analyzed using the community AMS analysis software SQUIRREL (version 1.51H) and PIKA (version 1.10H) as well as custom code written in Igor Pro (version 6, WaveMetrics Inc., USA).

2.3 Particle sources

Five types of rBC particles were produced in the laboratory by combustion, spark-generation or nebulization of commer-

cial samples. A sixth sample was measured directly behind an aircraft turbine at a commercial turbine servicing facility (SR Technics, Zurich Airport, Switzerland). Table 1 gives a summary of the measurement schedule.

2.3.1 CAST Black (CBK) and CAST Brown (CBW)

A combustion aerosol standard burner (CAST, model 00-4, Jing Ltd., Zollikofen, Switzerland) produced particles via a propane diffusion flame. Manufacturer characterization has been published online at http://www.sootgenerator.com/publ. htm. The CAST burner was used to produce two types of particles. The first type, referred to as CAST "Black" (CBK), was produced at a fuel-equivalence ratio $\phi = 0.85$ (carbon-to-oxygen ratio C/O = 0.25), and contained little organic matter. The second type, referred to as CAST "Brown" (CBW) after its visual appearance on a filter, was produced by a fuel-rich flame ($\phi = 1.36$; C/O = 0.41) and contained significant amounts of OM (Fig. S2). Additional experiments were performed with CBW after thermodenuding at 250 °C. Denuding reduced the organic mass to near-detection-limit for the AMS.

2.3.2 GFG spark-generated particles (GFG)

A PALAS GFG 1000 spark generator (Helsper et al., 1993) produced carbonaceous particles by repeated electrical discharge across graphite electrodes. The PALAS GFG generator was sparked at 75 Hz in an argon atmosphere (grade 6.0), with no additional dilution. GFG particles are morphologically similar to diesel particles (Weingartner et al., 1995; Burtscher, 2005; Schneider et al., 2006), although their microstructure and chemistry are significantly different (Saathoff et al., 2003; Schmid et al., 2011).

2.3.3 Regal Black (RB)

Regal Black (Cabot REGAL R400 pigment black), a carbon black distributed by Cabot Corp., USA, is the recommended calibration standard for the SP-AMS (Onasch et al., 2012). A sample of Regal Black from lot no. GP-3901 was received from Aerodyne Research Inc. to ensure consistency. The RB sample was suspended in Milli-Q water and nebulized with

grade 5.6 synthetic air in a homebuilt Collison-type nebulizer, before drying within a silica gel diffusion dryer.

2.3.4 Fullerene-enriched particles (FS)

Fullerene-enriched carbonaceous particles were obtained from Sigma-Aldrich ("fullerene soot as produced", lot no. MKBB8240V). These particles are produced by resistive heating of graphite such that carbonaceous nanoparticles nucleate above the graphite surface (Krätschmer et al., 1990). When performed under $\sim 10\,\mathrm{kPa}$ helium, this process results in nanoparticles containing $\sim 7\,\mathrm{wt\%}$ fullerenes ($\sim 6\,\mathrm{wt\%}$ C_{60}, $\sim 1\,\mathrm{wt\%}$ C_{70}) (Sigma-Aldrich, personal communication, 2012). FS is commonly used to calibrate single-particle soot photometers (SP2) instruments, as its incandescence-to-rBC-mass response is similar to that of rBC in ambient and diesel exhaust particles (Moteki and Kondo, 2010; Laborde et al., 2012).

2.3.5 Aircraft gas-turbine engine emissions (TU)

In a separate experiment to the laboratory campaign, emissions from a civil aviation gas turbine were sampled directly behind the engine. The turbine, a CFM56-5B4-2P engine, is commonly used by modern, short-haul civilian aircraft. Turbine exhaust was sampled through an 8 mm inner diameter, stainless steel, single-point sampling probe. The probe occupied a single, fixed position directly within the engine exhaust stream. The measurements reported here were taken from an undiluted "ICAO Annex 16" industry-standard sampling line (Crayford, 2012) and represent fuel-rich combustion. Additional details on the sampling configuration and data analysis for TU are given in the Supplement (Sect. S7.3).

3 Results and discussion

The dual vaporizer configuration of the SP-AMS (Sect. 2.2) allowed the laser vaporizer to be switched periodically on or off while the thermal vaporizer remained continuously on. In laser-on mode, rBC particles are expected to vaporize within the laser, along with any internally mixed non-absorbing material volatile below 4000 K. In laser-off mode, only NR-PM is observed, which in this study was largely organic matter (OM). To distinguish between these two modes, we will refer to "SP-AMS" (laser on) and "AMS" (laser off) data, along with the terms rBC and OM.

The results presented here will focus on those mass-spectral signals present only with the SP-AMS laser on, i.e., the refractory component of the particles. All SP-AMS mass spectra contained carbon-ion clusters C_x^{n+} as the major signals. In general, these signals were negligible in AMS mass spectra, as shown by Fig. 2. The figure compares the AMS and SP-AMS signals at C_1^+ and C_3^+ on the lower ordinate. Two sequential monodisperse experiments are shown, at 200 and 305 nm. The upper ordinate shows that CPC num-
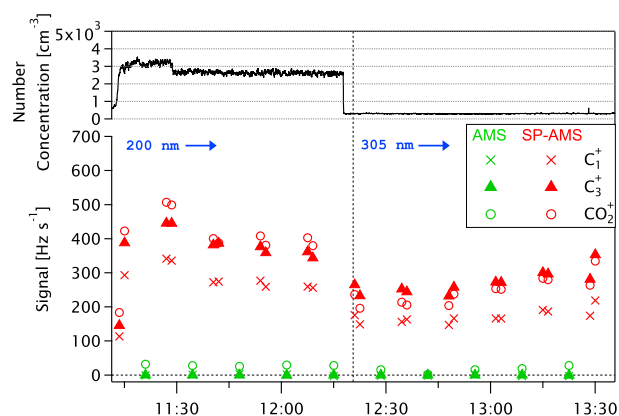

Fig. 2. Lower ordinate: time series of C_1^+ ($\times$), C_3^+ ($\triangle$), and CO_2^+ ($\circ$) for Regal Black during two size-selected experiments for AMS (green symbols) and SP-AMS (red symbols) measurements. Upper ordinate: CPC particle number concentration time series.

ber concentrations were stable throughout the period. While clear C_1^+ and C_3^+ signals were observed by the SP-AMS (red symbols), the AMS data (green) were at or below detection limit. These refractory C_x^{n+} signals are discussed in detail in Sect. 3.1.

In addition to C_x^{n+}, significant SP-AMS signals were detected from refractory particulate CO^+ and CO_2^+. Figure 2 additionally shows the time series of CO_2^+ in circle symbols on the lower ordinate. The signal clearly increases during SP-AMS measurement (red). Relative to C_x^+, a significant CO_2^+ signal remains in AMS periods. This is discussed in Sect. 3.2.

3.1 Carbon-cluster fragmentation patterns

The following subsections present a general description of each of the C_x^{n+} fragmentation patterns (Sect. 3.1.1) followed by an intercomparison of the C_x^+ patterns for the six samples (Sect. 3.1.2).

3.1.1 C_x^{n+} ions

For all six samples, carbon clusters containing 1 to 3 atoms (C_{1-3}^+) dominated the SP-AMS mass spectrum, as illustrated by Fig. 3. The figure shows the percentage contribution of C_{1-3}^+ to the total C_x^{n+} signal for $n = 1$ and $1 < x < 16$ (C_{1-16}^+). In total, C_{1-3}^+ made up 60–85 % of the C_{1-16}^+ signal depending on the sample. The two ions C_1^+ and C_3^+ each contributed at least 30 % of C_{1-16}^+ for all samples. For C_2^+, the contributions ranged from 3–18 %. This is consistent with the expected higher stability of odd-numbered, positively charged carbon clusters (Raghavachari and Binkley, 1987).

Carbon-cluster ions with $x > 16$ and $n > 1$ were observed for three samples: GFG, CBW, and, especially, FS. Since in general these signals were highest for FS, we believe that they originated from pre-existing fullerene molecules within the rBC particles. However, our data do not rule out the
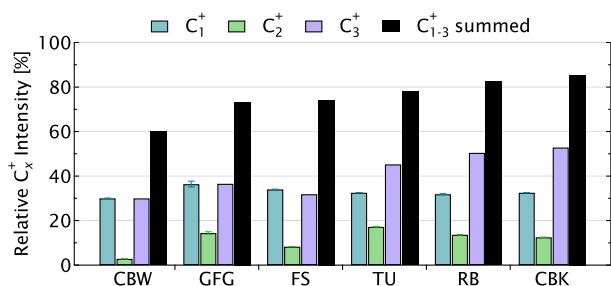
Fig. 3. Percentage contribution of C_{1-3}^+ ions to the sum of C_x^+ signals ($1 < x < 16$) for CAST "Brown" (CBW), spark-generated particles (GFG), fullerene-enriched soot (FS), aircraft-turbine particles (TU), Regal Black (RB), and CAST "Black" (CBK), in order of increasing C_{1-3}^+ intensity. Error bars for C_1^+ to C_3^+ are propagated from Poisson ion counting statistics. The data represent an average over all selected sizes.

possibility that fullerenes, or simply larger carbon clusters, may form within the instrument during particle vaporization. Previous work by Onasch et al. (2012) also identified significant signals at $C_{x>16}^+$ originating from a sample of denuded flame soot. They attributed signals above m/z 384 to fullerenes, and smaller ions to linear or ring structures.

For all samples presented here, peaks at $C_{x>16}^+$ were generally less intense than peaks at $C_{x<6}^+$. For example, for FS the most intense peak above the mass-to-charge ratio of C_{16}^+ (m/z 192) was at m/z 216, and was only 2.6 % as intense as the peak at m/z 36. Moreover, this m/z 216 peak included signals from not only C_{18}^+, but also from C_{36}^{2+} and C_{54}^{3+}. The presence of these multiply charged ions was evidenced by the isotope peaks $^{13}C_1{}^{12}C_{35}^{2+}$ (m/z 216.50), $^{13}C_1{}^{12}C_{54}^{3+}$ (216.33) and $^{13}C_2{}^{12}C_{53}^{3+}$ (216.66). No other multiply charged peaks were present at m/z 216.00, as confirmed by the absence of significant $^{13}C_1{}^{12}C_{71}^{4+}$ signal at m/z 216.25. The peak areas of $^{13}C_1{}^{12}C_{35}^{2+}$ and $^{13}C_1{}^{12}C_{54}^{3+}$ could therefore be combined with the isotopic abundance of $^{13}C_1$ to estimate the contributions of C_{18}^+, C_{36}^{2+}, and C_{54}^{3+} to m/z 216.00 (Fig. S3). We found that C_{36}^{2+} contributed the majority of the signal at m/z 216.00, representing 62.8 ± 0.8 % of the total. Of the remainder, the majority was due to C_{18}^+ (33.1 ± 0.6 %). C_{54}^{3+} contributed only 4.1 ± 0.6 %. Extrapolating this result to all $C_{x>16}^+$ peaks suggests that fullerene ions dominated the high-m/z range, although ring structures were present in non-negligible amounts. This is in contrast to Onasch et al. (2012), who did not report multiply charged ions.

A high intensity of multiply charged C_x^{n+} ions is expected for fullerenes – which exist for $C_{x>30}$ (von Helden et al., 1993) – due to their unique electronic and geometric structure (Scheier et al., 1994; Matt et al., 1996). However, ring- or linear-shaped carbon clusters at $C_{x<36}$ may also acquire multiple charges. In the FS mass spectrum discussed above, we observed multiply charged C_3 via the iso-

tope ion $^{13}C_1{}^{12}C_2^{2+}$ at m/z 18.050. This ion indicated that C_3^{2+} was present at only 5 % of the C_3^+ intensity. This is consistent with the much higher energy required to form smaller, doubly charged C_x^{n+} ions (Díaz-Tendero et al., 2002; Zimmerman et al., 1991). The relative intensity of multiply charged ions is therefore low for smaller C_x^+ ions, but high for fullerenes. Because of the potential for misinterpreting these multiply charged fullerene ions, and potential differences in their production between instruments, their abundance should be checked in future SP-AMS studies.

In order to present carbon-cluster mass spectra for higher x, we restricted the present analysis to nominally singly charged C_x^+ ions with $1 < x < 16$ (m/z 12–200) and their corresponding $^{13}C_1C_{x-1}^+$ daughters. This may include interferences from multiply charged C_x^{n+} with $m/z = 12n$, along with $^{13}C_2{}^{12}C_{x-2}^{2n+}$ isotope ions. The C_x^+ mass spectra for all samples are given in Figs. S4–S9. Constraining the present discussion to C_{1-16}^+ allows a representation of the highest-intensity ions while avoiding ambiguity for CBW, where significant PAH signals at high m/z (> 200) were difficult to distinguish from C_x^{n+} signals in our mass spectra. We will below refer to the set of considered ions as C_x^+.

3.1.2 C_1^+/C_3^+ to distinguish rBC types

Given that C_1^+ and C_3^+ represented the majority of the C_x^+ signal from all six samples, and that C_x^+ represented the majority of SP-AMS signals, this section explores the possibility of using these two ions as markers to distinguish between different sources of rBC based on their carbon-cluster fragments.

The ratio of signal intensities at C_1^+ and C_3^+ are plotted in Fig. 4 for all samples and mobility diameters listed in Table 1. The figure shows the 25th to 75th percentile as a box, with whiskers extending to the 10th and 90th percentile. The horizontal line across each box represents the median. The data include a large range of signal intensities: ion rates for GFG were a factor of 20 lower than for CBW, while CBK ion rates were a factor of 3 higher. The samples fall broadly into two categories, with FS, GFG, CBW and CBWTD all having C_1^+/C_3^+ close to 1, while TU, RB and CBK each have $C_1^+/C_3^+ < 0.8$. The range of values for TU is especially narrow due to the fact that one stable engine condition is presented, as described in Sect. S7.3 of the Supplement. In order to verify that the C_1^+/C_3^+ ratio is reproducible, we compared our RB C_1^+/C_3^+ ratio to that measured using a different instrument at Aerodyne Research Inc. but the same RB sample (Onasch et al., 2012). Onasch et al. observed a C_1^+/C_3^+ ratio of 0.63 (○ in Fig. 4). The present data have a mean C_1^+/C_3^+ ratio of 0.67 (× in Fig. 4), indicating that the C_1^+/C_3^+ ratio may be a reproducible characteristic of this sample.
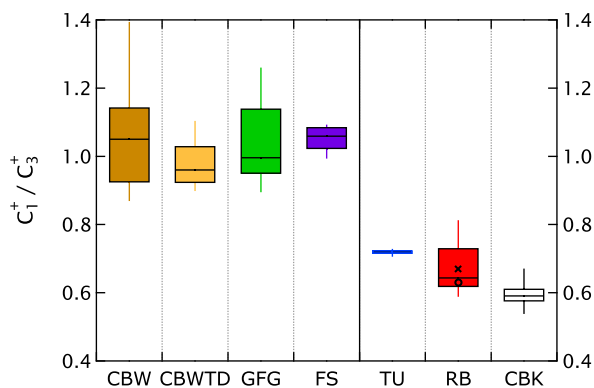
Fig. 4. SP-AMS C_1^+/C_3^+ ratios for CAST "Brown" particles (CBW), thermodenuded CBW (CBWTD), spark-generated particles (GFG), fullerene-enriched soot (FS), aircraft-turbine particles (TU), Regal Black (RB), and CAST "Black" particles (CBK). All samples were monodisperse particles at multiple sizes, except TU. Each box spans the 25th to 75th percentile. Vertical lines extend to the 10th and 90th percentiles. The horizontal line within each box shows the median. The mean C_1^+/C_3^+ ratio for RB is shown for the present study ($\times$) and for independent measurements by Onasch et al. ($\circ$).

We next hypothesized that the C_1^+/C_3^+ ratio may depend on the chemical structure of the rBC, and compared the C_x^+ mass spectra of each sample relative to FS. FS was chosen as a reference since it is commercially available, commercially traceable, and gave high-intensity signals at a large m/z range. Figure 5 shows the C_x^+ spectral intensity for each sample plotted against FS on a log-log scale. Each spectrum is normalized to unity and excludes isotope ions for clarity. Since all spectra were dominated by C_{1-3}^+ (Sect. 3.1.1), these ions are found near the top-right corner, as labeled in white for RB. The white labels also apply to all data points vertically above or below the RB data points. Ions C_{4-5}^+ lie near to each other. None of the signals for $C_{\geq 6}^+$ were greater than 0.1 % (10^{-3}) of the C_x^+ signal for RB, TU, or CBK.

Figure 5 shows that the six mass spectra are grouped into the same two categories as the C_1^+/C_3^+ ratios in Fig. 4. The mass spectra of GFG and CBW fall near the 1 : 1 line and are therefore similar to FS. In contrast, TU, RB, and CBK are generally shifted downwards, due to the lower relative intensities of heavier ions. The C_x^+ spectra of FS, GFG, and CBW all contain significant signals up to and beyond C_{16}^+, while TU, RB, and CBK were dominated by the smaller C_{1-5}^+ clusters. For TU, RB and CBK, the contribution of C_x^+ ions with $x \geq 6$ was always less than 0.1 % of the total C_x^+. This absence was not due to a lack of sufficient signal: the CBK mass spectrum was obtained at signal intensities a factor of 60 higher than for GFG.
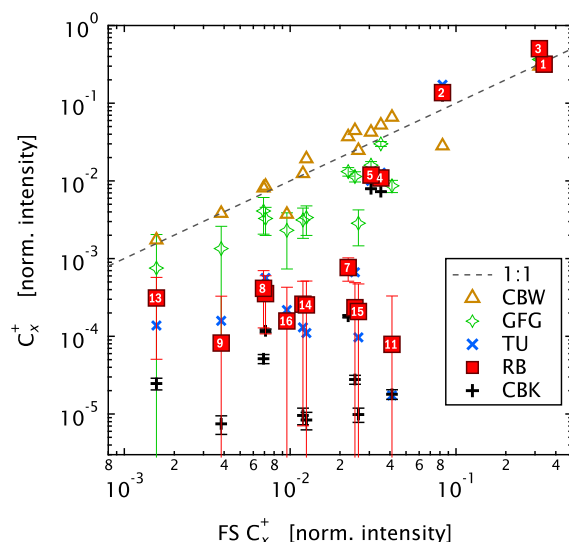

Fig. 5. Scatterplot of mass spectral intensities at each C_x^+ up to $x = 16$. All spectra are normalized to unity and plotted against the FS C_x^+ spectrum. The white numbers labeling RB (red squares) indicate the number of carbon atoms x in each C_x^+ for both RB and FS. For clarity, some labels have been omitted, namely C_x^+ with $x = 6$ (next to 8), 12 (next to 14), and 10 (next to 15). Error bars indicate ion counting uncertainties, and are not shown when they are smaller than the data symbols.

3.1.3 Atmospheric suitability of C_1^+/C_3^+

Minor quantities of C_1^+ and C_3^+ can be produced by organic molecules in the AMS and SP-AMS. These signals are typically negligible when compared to the overall AMS mass spectrum (e.g., Alfarra, 2004), but may be sufficient to interfere with C_x^+ signals from rBC during atmospheric sampling when organic mass fractions are high.

Since an organic molecule is more likely to form C_1^+ ions than C_3^+ ions, OM interference would be expected to artificially enhance the C_1^+/C_3^+ ratio, thus potentially limiting the usefulness of the C_1^+/C_3^+ ratio to distinguish between rBC sources. A simplistic solution to this problem for the dual-vaporizer setup used here would be subtraction of the AMS C_x^+ signal from the SP-AMS C_x^+ signal. However, this may not be appropriate; Onasch et al. (2012) have observed a different fragmentation pattern when dioctyl sebacate was vaporized by AMS, compared to vaporization by SP-AMS after coating on glassy-carbon rBC spheres.

We tested the possibility of organic interference in our analysis by removing OM from CBW with a thermodenuder at $250\,°C$ prior to size selection. After thermodenuding, the AMS organic signal for 305 nm CBW particles was reduced to near-detection limit (Fig. S2), whereas the C_1^+/C_3^+ ratio did not change appreciably (Fig. 4).

CBW had the highest OM content (based on the relative signal of AMS organics to C_x^+ ions) of the laboratory samples

discussed herein. Nevertheless, C_1^+ signals were a factor of 250 lower in the AMS than in the SP-AMS for 305 nm non-thermodenuded CBW particles, and fell below detection limit for thermodenuded 305 nm CBW particles. A factor of 250 is large but not insignificant: the corresponding spherical-equivalent diameters required for a 1 : 1 AMS:SP-AMS signal ratio at C_1^+ are approximately 50 nm for a CBW "core" and 440 nm for CBW organic matter, assuming respective material densities of 1.8 g cm^{-3} (Park et al., 2004) and 1.3 g cm^{-3} (Slowik et al., 2007). The CBW OM was dominated by PAHs (Fig. S2), which may have a C_1^+ yield different to that of typical ambient OM. However, this estimation indicates that OM mixed with rBC in ambient studies may significantly interfere with the determination of C_1^+/C_3^+ from ambient rBC.

To avoid such interference, either organic material may be thermodenuded prior to sampling, or a different marker using higher-mass C_x^+ may be useful. All samples in the present study yielded carbon clusters C_{1-5}^+. Considering all possible combinations of C_{1-5}^+, we found that C_4^+/C_3^+ is probably the best alternative ratio when organic interferences are significant (Fig. S10). Like C_1^+/C_3^+, this ratio also distinguishes between particle sources according to their C_x^+ mass spectra. The disadvantage of this ratio is its relatively lower limit of quantification: since fewer C_4^+ ions than C_1^+ ions are produced per unit mass of rBC vaporized, a higher rBC mass would be required to determine C_4^+/C_3^+ rather than C_1^+/C_3^+. Additional studies using a variety of organic coatings should be performed to investigate whether such coatings influence these ratios.

3.2 Refractory CO_x^+ signals (rCO_x)

3.2.1 Identification of rCO_x

In addition to C_x^{n+}, SP-AMS signals included oxygen-containing ions such as CO_2^+, CO^+, H_2O^+, OH^+, and O^+, which we refer to as rCO_x. Because similar ions may also form from OM (both refractory and non-refractory), the identification and understanding of these signals is important for the interpretation of SP-AMS measurements from unknown samples. In this section, we discuss rCO_x signals from RB. The focus is on CO_2^+ and CO^+, since these ions could not have resulted from the ionization of residual water on the particles. We focus on RB as a model sample because its C_x^{n+} mass spectrum was dominated by the singly charged ions C_{1-5}^+, simplifying its interpretation (Sect. 3.1.1). Additionally, RB is the recommended calibration standard for the SP-AMS (Onasch et al., 2012).

The refractory nature of rCO_x is illustrated by Fig. 6. The figure plots the PToF spectrum at m/z 28 (N_2^+ or CO^+) for both AMS (green) and SP-AMS (red) operating modes while sampling polydisperse RB particles. The SP-AMS PToF spectrum of m/z 36 (C_3^+, black symbols) is shown for reference. Symbols represent raw data, while
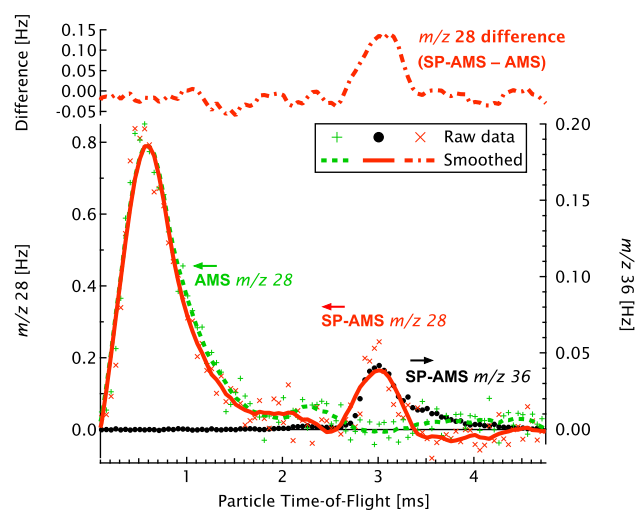

Fig. 6. Signal at m/z 28 (N_2^+ or CO^+) and m/z 36 (C_3^+) as a function of particle time-of-flight for polydisperse RB particles. Data symbols show the raw SP-AMS or AMS data, which have been smoothed by a Savitsky–Golay filter for clarity when the signal-to-noise was low (curves). The first peak (0.6 ms) corresponds to gas-phase N_2, the second (3 ms) to CO^+ originating from the RB particles. The upper panel (dash-dotted line) shows the difference of the SP-AMS and AMS curves.

curves represent smoothed data (using a 4th-order, 25-point Savitsky–Golay filter to preserve peak shape). Both the red SP-AMS and green AMS m/z 28 curves show a strong peak from gas-phase N_2, at approximately 0.6 ms. However, only the SP-AMS shows a second peak at 3 ms. This peak is clearly within the particle phase, and corresponds to a mode vacuum-aerodynamic diameter of 386 ± 1 nm. This second peak is coincident with the arrival of the RB particles, as demonstrated by the coincident peak at m/z 36. We infer that the second m/z 28 peak at 3 ms most likely originated from CO^+ formed when the rBC was vaporized.

The peak at m/z 36 is broad and possibly bimodal, whereas the peak at m/z 28 appears to decrease faster than at m/z 36. This suggests that the refractory CO^+ content of RB is a function of particle size. A size dependence is also indicated by a decreasing ratio of CO_2^+ to C_3^+ with increasing mobility diameter for size-selected experiments. In these experiments, the CO_2^+/C_3^+ ratio decreased from 1.6 (125 nm) to 0.8 (500 nm). The PToF signal at m/z 44 (CO_2^+) also peaked simultaneously with m/z 36 (C_3^+) (Fig. S11), demonstrating its particulate origin as previously observed by Onasch et al. (2012).

The relative significance of rCO_x was estimated by comparing the areas of log-normal curves fitted to the polydisperse PToF spectra. Bimodal fits were used for particulate m/z 36 (C_3^+) and m/z 44 (CO_2^+). The estimated CO_2^+/C_3^+ ratio was 1.0, consistent with the ratio found from the size-selected measurements. The corresponding CO^+/C_3^+ ratio was estimated as 20, but may be positively biased by

interference from N_2^+. Furthermore, this ratio cannot be interpreted as a direct mass ratio before accounting for the ionization efficiencies of both C_x^+ and rCO_x^+. When accounting for C_x^+ and not rCO_x, the ionization efficiency of RB is 0.1 (Onasch et al., 2012), suggesting that a mass-weighted CO^+/C_3^+ ratio may be lower. For a mass-weighted ratio, the ionization efficiencies of both C_x^+ and rCO_x must be known. Nevertheless, such a high ratio indicates clearly that rCO_x species are an important component of RB.

Significantly higher PToF signals in the SP-AMS than the AMS were also observed at other m/z such as 18 (H_2O^+), 17 (OH^+) and 16 (O^+) for RB. Furthermore, significant rCO_x signals were also observed for every sample discussed above. The potential origin and significance of these signals are discussed in the next section.

3.2.2 Origin of rCO_x^+

The observation of increased rCO_x^+ within the SP-AMS relative to the AMS mass spectrum could be due to (1) oxygenated functional groups incorporated into the refractory structure of the rBC, (2) fragmentation of refractory OM, (3) CO or CO_2 adsorbed to the particle surface, (4) gaseous CO or CO_2 trapped within internal voids, or (5) reaction of carbon vapor with gas-phase O_2. This section will argue that the first possibility is the most likely, and discuss the implications.

The second possibility is unlikely, since the SP-AMS mass spectrum of RB did not contain significant signals from hydrocarbon ions ($C_xH_y^+$, $C_xH_yO^+$, etc.) even though the signal intensity of rCO_2^+ was close to that of C_3^+ in the RB mass spectrum. Thus, any refractory organic molecules would have to include a negligible contribution of carbon-hydrogen bonds, while simultaneously being large enough to be non-volatile at 600 °C. Moreover, for RB, these molecules would have had to form during its industrial production from hydrocarbon oils at 1500 °C. This combination of properties is physically unreasonable.

The third and fourth possibilities are not likely to be the major source of rCO_x in RB. Desorption of adsorbed CO_2 is expected to occur within minutes (Sevilla and Fuertes, 2011). The 30 min residence chamber used in the current experiments should have provided sufficient time for desorption after nebulizing in CO_2-free gas (Sect. 2.1). Voids within RB particles containing CO_2(g), would contain very little CO_2 mass per particle, since the density of CO_2(g) is a factor of 1000 smaller than that of rBC, yet the observed CO_2^+/C_3^+ ratio was 0.8–1.6. Finally, the fifth possibility would yield C_xO^+ and not CO_2^+ as the major product (von Helden et al., 1993). Such ions were not observed. Therefore, only the first possibility can be the major source of the observed rCO_x.

Oxygenated moieties incorporated into the refractory carbon structure of RB are expected based on its production method. RB is produced by atomizing a proprietary oil within a furnace at 1800 K, resulting in a "carbon black" that con-

tains only 0.5–1 wt% of material volatile at 1223 K. This carbon black is then treated with an unspecified, HNO_3-like acid (Cabot Corp., personal communication, 2013), likely at elevated temperatures (Otake and Jenkins, 1993), in order to increase surface functionalization. This increased functionalization is indicated by an increase in the percentage of mass volatile at 1223 K, from 0.5–1 wt% to 3.5 wt%.

The acid treatment of rBC yields oxygenated moieties including hydroxyl, carbonyl, carboxyl, lactone, and acid anhydride groups, depending on the reaction time (Sellitti et al., 1990; Vinke et al., 1994; Figueiredo et al., 1999, 2007). These groups thermally decompose into CO or CO_2 when heated slowly ($\sim 5\,K\,min^{-1}$) under inert atmospheres, typically at 500–1200 K depending on the functional group and heating rate (Zielke et al., 1996; Figueiredo et al., 1999, 2007). The thermal decomposition of such rBC surface groups should therefore be expected in the SP-AMS. The decomposition temperature of oxygenated moieties also relates to possibility (3) above: if such moieties decompose at 500–1200 K, then no distinction between refractory, adsorbed CO_2(g) and chemically bonded moieties can be made.

3.2.3 Atmospheric relevance of rCO_x^+

In an atmospheric context, oxygenated surface groups may feasibly form via reaction with oxidants such as O_2 (Otake and Jenkins, 1993; Figueiredo et al., 1999), ozone (e.g., McCabe and Abbatt, 2008) as well as other atmospheric oxidants (Saathoff et al., 2001). Oxidation is likely to occur within the combustion region where rBC is produced (Frenklach, 2002). In the present study, the presence of rCO_x in the propane-flame samples, CBK and CBW, indicates the potential real-world significance of these SP-AMS species, even in the absence of further aging. Other real-world sources of rCO_x, such as metal-oxide fuel additives (Bladt et al., 2012), may also be significant to SP-AMS measurements.

The atmospheric significance of the oxidized surface species which likely lead to rCO_x signals must be considered in context of the overall aerosol. In general, combustion sources emit organic material in addition to rBC. This organic matter is emitted in both the particulate (OM) and the gas phase, and represents a major contribution to the overall composition of the particle. For example, Bond et al. (2013) have recently estimated OM-to-BC ratios between 1 and 10 for primary emissions. After emission, this ratio is likely to increase significantly due to condensation of atmospherically oxidized gas-phase organic compounds. For example, diesel-engine OM may increase two-fold after a few hours of moderate atmospheric aging (Robinson et al., 2007), and less efficient processes such as wood combustion may increase OM by seven-fold under similar conditions (e.g., Heringa et al., 2011). These oxidation timescales (hours) are considerably shorter than the atmospheric lifetime of rBC (days) and produce highly oxidized OM (e.g., Jimenez et al., 2009). Further, coagulation with pre-existing particles also occurs on

a short timescale (tens of hours) relative to the rBC atmospheric lifetime. Overall, for a global average, neither the bulk nor the surface properties of rBC are expected to be dominated by rCO_x.

On the regional scale, fresh rBC particles can represent a significant portion of the aerosol near sources, for example within cities (e.g., Seinfeld and Pandis, 2012). These particles may contain a significant fraction of OM, possibly reducing the significance of rCO_x to their overall chemistry. In the absence of OM, freshly-emitted rBC particles have been measured as cloud-condensation-nucleus inactive (e.g., Kuwata et al., 2009), so rCO_x species are apparently not able to initiate droplet activation on such particles.

Conversely, freshly emitted combustion particles are expected to play a significant role in heterogeneous chemistry, for example, reducing ozone or nitrogen dioxide (NO_2) (McCabe and Abbatt, 2008; Han et al., 2013). Han et al. (2013) found that preheating n-hexane soot to 573 K significantly decreased the uptake of NO_2, indicating that volatile OM was the primary reactant. Furthermore, the yield of gas-phase products simultaneously changed upon heating, indicating that the OM shielded the rBC surface from oxidation. From these results, one may propose that when a freshly produced rBC particle is coated by OM the rBC reactivity may become slow enough that rCO_x could be used as a chemical tracer. For example, the ratio CO_2^+/C_3^+ of an OM-denuded rBC particle may be useful in source apportionment studies. However, this extrapolation must be verified by future laboratory studies using different primary and secondary OM samples. If this hypothesis is proven false, and rCO_x does in fact increase with atmospheric oxidation, then this SP-AMS signal may be useful in tracking the atmospheric age of rBC.

Finally, rCO_x may be significant for SP-AMS calibration. Neglecting rCO_x during calibration would not only give an inaccurate sensitivity factor, but would lead to the misquantification of rBC with different degrees of oxidation. Although the elemental analysis of acid-treated rBC by Figueiredo et al. (1999) suggests an error on the order of 10 %, the estimated signal from CO^+ in Sect. 3.2.1, suggests that the SP-AMS error may be much higher.

4 Summary

SP-AMS mass spectra showed just two different overall carbon fragmentation patterns for six rBC samples generated by a variety of methods, from aircraft-turbine combustion to propane flame combustion to spark vaporization. One group of samples yielded carbon-cluster ions ranging up to a few hundred m/z. The other group gave carbon-cluster mass spectra which did not extend appreciably beyond C_5^+. The two groups could be distinguished according to the ratio C_1^+/C_3^+, which was approximately 1 for the former group and less than 0.8 for the latter.

Two ion ratios were identified for source apportionment, when an air mass contains a mixture of rBC from the two C_x^{n+} categories. The first ratio, C_1^+/C_3^+, maximizes the rBC detection limit by using the two most intense C_x^{n+} peaks in the mass spectrum. In this case, thermodenuding of the rBC sample prior to measurement is recommended due to possible interference by the trace amounts of C_1^+ produced during the fragmentation of OM ions. The second ratio, C_4^+/C_3^+, aims to avoid this interference by using higher-mass C_x^{n+} ions. The sensitivity of C_4^+/C_3^+ to an OM coating was tested using a PAH-rich propane-flame sample (CBW). Further tests with thicker coatings and different chemicals should be performed.

In addition to C_x^{n+} ions, the SP-AMS mass spectrum of all six samples included oxygenated ions. These ions most likely originated from the thermal decomposition of oxygenated moieties within the refractory carbon structure. Their quantification was hindered by high signals from gas-phase molecules such as N_2^+.

It is not clear whether or not these refractory oxygenated moieties play a role in the heterogeneous chemistry of atmospheric combustion particles. If so, their quantification by SP-AMS could provide a useful measurement of rBC age. If not, they may be inert enough to allow their SP-AMS signals to be used in source apportionment, since different sources will produce different amounts of oxygenated moieties following differences in the combustion process.

Future work should aim to quantify these ions for a number of samples, also as a function of atmospheric age, to provide a basis for the interpretation of ambient SP-AMS spectra in which gas-phase interferences by N_2^+ are unavoidable. Further studies might also investigate whether the SP-AMS is capable of providing enough information to distinguish between different refractory functional groups, as has been done using well-established offline techniques.

Supplementary material related to this article is available online at http://www.atmos-chem-phys.net/14/2591/2014/acp-14-2591-2014-supplement.pdf.

References

Alfarra, M. R.: Insights Into Atmospheric Organic Aerosols Using An Aerosol Mass Spectrometer, Ph.D. Thesis, Department of Chemical Engineering, University of Manchester, 2004.

Bladt, H., Schmid, J., Kireeva, E. D., Popovicheva, O. B., Persentseva, N. M., Timofeev, M. A., Heister, K., Uihlein, J., Ivleva, N. P., and Niessner, R.: Impact of Fe content in laboratory-produced soot aerosol on its composition, structure, and thermo-chemical properties, Aerosol Sci. Tech., 46, 1337–1348, 2012.

Bond, T. C., Doherty, S. J., Fahey, D. W., Forster, P. M., Berntsen, T., DeAngelo, B. J., Flanner, M. G., Ghan, S., Kärcher, B., Koch, D., Kinne, S., Kondo, Y., Quinn, P. K., Sarofim, M. C., Schultz, M. G., Schulz, M., Venkataraman, C., Zhang, H., Zhang, S., Bellouin, N., Guttikunda, S. K., Hopke, P. K., Jacobson, M. Z., Kaiser, J. W., Klimont, Z., Lohmann, U., Schwarz, J. P., Shindell, D., Storelvmo, T., Warren, S. G., and Zender, C. S.: Bounding the role of black carbon in the climate system: A scientific assessment, J. Geophys. Res., 118, 5380–5552, doi:10.1002/jgrd.50171, 2013.

Burtscher, H.: Physical characterization of particulate emissions from diesel engines: a review, J. Aerosol Sci., 36, 896–932, 2005.

Canagaratna, M., Jayne, J., Jimenez, J., Allan, J., Alfarra, M., Zhang, Q., Onasch, T. B., Drewnick, F., Coe, H., Middlebrook, A., Delia, A., Williams, L., Trimborn, A., Northway, M., DeCarlo, P., Kolb, C., Davidovits, P., and Worsnop, D.: Chemical and microphysical characterization of ambient aerosols with the aerodyne aerosol mass spectrometer, Mass Spectrom. Rev., 26, 185–222, doi:10.1002/mas.20115, 2007.

Cape, J. N., Coyle, M., and Dumitrean, P.: The atmospheric lifetime of black carbon, Atmos. Environ., 59, 256–263, doi:10.1016/j.atmosenv.2012.05.030, 2012.

Cappa, C. D., Onasch, T. B., Massoli, P., Worsnop, D. R., Bates, T. S., Cross, E. S., Davidovits, P., Hakala, J., Hayden, K. L., and Jobson, B. T.: Radiative absorption enhancements due to the mixing state of atmospheric black carbon, Science, 337, 1078–1081, 2012.

Cappa, C. D., Onasch, T. B., Massoli, P., Worsnop, D. R., Bates, T. S., Cross, E. S., Davidovits, P., Hakala, J., Hayden, K. L., and Jobson, B. T.: Response to Comment on "Radiative absorption enhancements due to the mixing state of atmospheric black carbon", Science, 339, 393–393, 2013.

Corbin, J., Rehbein, P., Evans, G., and Abbatt, J.: Combustion particles as ice nuclei in an urban environment: evidence from single-particle mass spectrometry, Atmos. Environ., 51, 286–292, 2012.

Crayford, A., Johnson, M., Marsh, R., Secvenco, Y., Walters, D., Williams, P., Petzold, A., Bowen, P., Wang, J., and Lister, D.: SAMPLE III: Contribution to aircraft engine PM certification requirement and standard, Second Specific Contract, Final Report, European Aviatian Safety Agency, Cologne, Germany, 2012.

DeMott, P. J., Chen, Y., Kreidenweis, S. M., Rogers, D. C., and Sherman, D. E.: Ice formation by black carbon particles, Geophys. Res. Lett., 26, 2429–2432, doi:10.1029/1999gl900580, 1999.

Díaz-Tendero, S., Martín, F., and Alcamí, M.: Structure, Dissociation Energies, and Harmonic Frequencies of Small Doubly Charged Carbon Clusters $C^n 2+ (n = 3–9)$, J. Phys. Chem. A, 106, 10782–10789, 2002.

Engelhart, G. J., Hennigan, C. J., Miracolo, M. A., Robinson, A. L., and Pandis, S. N.: Cloud condensation nuclei activity of fresh primary and aged biomass burning aerosol, Atmos. Chem. Phys., 12, 7285–7293, doi:10.5194/acp-12-7285-2012, 2012.

Figueiredo, J., Pereira, M., Freitas, M., and Orfao, J.: Modification of the surface chemistry of activated carbons, Carbon, 37, 1379–1389, 1999.

Figueiredo, J. L., Pereira, M. F., Freitas, M. M., and Órfão, J. J.: Characterization of active sites on carbon catalysts, Ind. Eng. Chem. Res., 46, 4110–4115, 2007.

Flanner, M. G., Zender, C. S., Randerson, J. T., and Rasch, P. J.: Present-day climate forcing and response from black carbon in snow, J. Geophys. Res., 112, D11202, doi:10.1029/2006JD008003, 2007.

Frenklach, M.: Reaction mechanism of soot formation in flames, Phys. Chem. Chem. Phys., 4, 2028–2037, 2002.

Gysel, M., Laborde, M., Mensah, A. A., Corbin, J. C., Keller, A., Kim, J., Petzold, A., and Sierau, B.: Technical Note: The single particle soot photometer fails to reliably detect PALAS soot nanoparticles, Atmos. Meas. Tech., 5, 3099–3107, doi:10.5194/amt-5-3099-2012, 2012.

Han, C., Liu, Y., and He, H.: Role of Organic Carbon in Heterogeneous Reaction of NO_2 with Soot, Environ. Sci. Technol., 47, 3174–3181, 2013.

Healy, R. M., Sciare, J., Poulain, L., Crippa, M., Wiedensohler, A., Prévôt, A. S. H., Baltensperger, U., Sarda-Estève, R., McGuire, M. L., Jeong, C.-H., McGillicuddy, E., O'Connor, I. P., Sodeau, J. R., Evans, G. J., and Wenger, J. C.: Quantitative determination of carbonaceous particle mixing state in Paris using single-particle mass spectrometer and aerosol mass spectrometer measurements, Atmos. Chem. Phys., 13, 9479–9496, doi:10.5194/acp-13-9479-2013, 2013.

Helsper, C., Mölter, W., Löffler, F., Wadenpohl, C., Kaufmann, S., and Wenninger, G.: Investigations of a new aerosol generator for the production of carbon aggregate particles, Atmos. Environ., 27, 1271–1275, doi:10.1016/0960-1686(93)90254-V, 1993.

Heringa, M. F., DeCarlo, P. F., Chirico, R., Tritscher, T., Dommen, J., Weingartner, E., Richter, R., Wehrle, G., Prévôt, A. S. H., and Baltensperger, U.: Investigations of primary and secondary particulate matter of different wood combustion appliances with a high-resolution time-of-flight aerosol mass spectrometer, Atmos. Chem. Phys., 11, 5945–5957, doi:10.5194/acp-11-5945-2011, 2011.

Hitzenberger, R., Giebl, H., Petzold, A., Gysel, M., Nyeki, S., Weingartner, E., Baltensperger, U., and Wilson, C.: Properties of jet engine combustion particles during the PartEmis experiment. Hygroscopic growth at supersaturated conditions, Geophys. Res. Lett., 30, 1779, doi:10.1029/2003GL017294, 2003.

IPCC: Contribution of Working Group I to the Fourth Assessment Report of the Intergovernmental Panel on Climate Change, edited by: Solomon, S., Qin, D., Manning, M., Chen, Z., Marquis, M., Averyt, K. B., Tignor, M., and Miller, H. L., Cambridge University Press, UK and New York, NY, USA, 2007.

Jacobson, M. Z.: Comment on "Radiative absorption enhancements due to the mixing state of atmospheric black carbon", Science, 339, 393–393, 2013.

Jayne, J. T., Leard, D. C., Zhang, X., Davidovits, P., Smith, K. A., Kolb, C. E., and Worsnop, D. R.: Development of an aerosol mass spectrometer for size and composition analysis of submicron particles, Aerosol Sci. Tech., 33, 49–70, doi:10.1080/027868200410840, 2000.

Jeong, C.-H., Herod, D., Dabek-Zlotorzynska, E., Ding, L., McGuire, M., and Evans, G.: Identification of the Sources and Geographic Origins of Black Carbon using Factor Analysis at Paired Rural and Urban sites, Environ. Sci. Technol., 47, 8462–8470, doi:10.1021/es304695t, 2013.

Jimenez, J. L., Jayne, J. T., Shi, Q., Kolb, C. E., Worsnop, D. R., Yourshaw, I., Seinfeld, J. H., Flagan, R. C., Zhang, X., Smith, K. A., Morris, J. W., and Davidovits, P.: Ambient aerosol sampling using the Aerodyne Aerosol Mass Spectrometer, J. Geophys. Res., 108, 8425, doi:10.1029/2001jd001213, 2003.

Jimenez, J. L., Canagaratna, M. R., Donahue, N. M., Prévôt, A. S. H., Zhang, Q., Kroll, J. H., DeCarlo, P. F., Allan, J. D., Coe, H., Ng, N. L., Aiken, A. C., Docherty, K. S., Ulbrich, I. M., Grieshop, A. P., Robinson, A. L., Duplissy, J., Smith, J. D., Wilson, K. R., Lanz, V. A., Hueglin, C., Sun, Y. L., Tian, J., Laaksonen, A., Raatikainen, T., Rautiainen, J., Vaattovaara, P., Ehn, M., Kulmala, M., Tomlinson, J. M., Collins, D. R., Cubison, M. J., Dunlea, E. J., J., Huffman, J. A., Onasch, T. B., Alfarra, M. R., Williams, P. I., Bower, K., Kondo, Y., Schneider, J., Drewnick, F., Borrmann, S., Weimer, S., Demerjian, K., Salcedo, D., Cottrell, L., Griffin, R., Takami, A., Miyoshi, T., Hatakeyama, S., Shimono, A., Sun, J. Y., Zhang, Y. M., Dzepina, K., Kimmel, J. R., Sueper, D., Jayne, J. T., Herndon, S. C., Trimborn, A. M., Williams, L. R., Wood, E. C., Middlebrook, A. M., Kolb, C. E., Baltensperger, U., and Worsnop, D. R.: Evolution of Organic Aerosols in the Atmosphere, Science, 326, 1525–1529, 2009.

Koehler, K. A., DeMott, P. J., Kreidenweis, S. M., Popovicheva, O. B., Petters, M. D., Carrico, C. M., Kireeva, E. D., Khokhlova, T. D., and Shonija, N. K.: Cloud condensation nuclei and ice nucleation activity of hydrophobic and hydrophilic soot particles, Phys. Chem. Chem. Phys., 11, 7906–7920, 2009.

Krätschmer, W., Fostiropoulos, K., and Huffman, D. R.: The infrared and ultraviolet absorption spectra of laboratory-produced carbon dust: evidence for the presence of the C_{60} molecule, Chem. Phys. Lett., 170, 167–170, 1990.

Kuwata, M., Kondo, Y., and Takegawa, N.: Critical condensed mass for activation of black carbon as cloud condensation nuclei in Tokyo, J. Geophys. Res., 114, D20202, doi:10.1029/2009JD012086, 2009.

Laborde, M., Mertes, P., Zieger, P., Dommen, J., Baltensperger, U., and Gysel, M.: Sensitivity of the Single Particle Soot Photometer to different black carbon types, Atmos. Meas. Tech., 5, 1031–1043, doi:10.5194/amt-5-1031-2012, 2012.

Liu, D., Allan, J., Whitehead, J., Young, D., Flynn, M., Coe, H., McFiggans, G., Fleming, Z. L., and Bandy, B.: Ambient black carbon particle hygroscopic properties controlled by mixing state and composition, Atmos. Chem. Phys., 13, 2015–2029, doi:10.5194/acp-13-2015-2013, 2013.

Martin, M., Tritscher, T., Jurányi, Z., Heringa, M. F., Sierau, B., Weingartner, E., Chirico, R., Gysel, M., Prévôt, A. S., and Baltensperger, U.: Hygroscopic properties of fresh and aged wood burning particles, J. Aerosol Sci., 56, 15–29, 2012.

Matt, S., Dünser, B., Lezius, M., Deutsch, H., Becker, K., Stamatovic, A., Scheier, P., and Märk, T.: Absolute partial and total cross-section functions for the electron impact ionization of C_{60} and C_{70}, J. Chem. Phys., 105, 1880–1896, 1996.

McCabe, J. and Abbatt, J.: Heterogeneous loss of gas-phase ozone on n-hexane soot surfaces: similar kinetics to loss on other chemically unsaturated solid surfaces, J. Phys. Chem. C, 113, 2120–2127, 2008.

Monge, M. E., D'Anna, B., Mazri, L., Giroir-Fendler, A., Ammann, M., Donaldson, D., and George, C.: Light changes the atmospheric reactivity of soot, P. Natl. Acad. Sci. USA, 107, 6605–6609, 2010.

Moteki, N. and Kondo, Y.: Dependence of laser-induced incandescence on physical properties of black carbon aerosols: measurements and theoretical interpretation, Aerosol Sci. Tech., 44, 663–675, doi:10.1080/02786826.2010.484450, 2010.

Onasch, T. B., Trimborn, A., Fortner, E. C., Jayne, J. T., Kok, G. L., Williams, L. R., Davidovits, P., and Worsnop, D. R.: Soot particle aerosol mass spectrometer: development, validation, and initial application, Aerosol Sci. Tech., 46, 804–817, doi:10.1080/02786826.2012.663948, 2012.

Otake, Y. and Jenkins, R. G.: Characterization of oxygen-containing surface complexes created on a microporous carbon by air and nitric acid treatment, Carbon, 31, 109–121, 1993.

Park, K., Kittelson, D. B., Zachariah, M. R., and McMurry, P. H.: Measurement of inherent material density of nanoparticle agglomerates, J. Nanopart. Res., 6, 267–272, 2004.

Petzold, A. and Schönlinner, M.: Multi-angle absorption photometry – a new method for the measurement of aerosol light absorption and atmospheric black carbon, J. Aerosol Sci., 35, 421–441, 2004.

Pratt, K. A. and Prather, K. A.: Mass spectrometry of atmospheric aerosols – recent developments and applications, Part II: On-line mass spectrometry techniques, Mass Spectrom. Rev., 31, 17–48, 2012.

Raghavachari, K. and Binkley, J.: Structure, stability, and fragmentation of small carbon clusters, J. Chem. Phys., 87, 2191–2197, 1987.

Ramanathan, V. and Carmichael, G.: Global and regional climate changes due to black carbon, Nat. Geosci., 1, 221–227, 2008.

Reilly, P. T. A., Lazar, A. C., Gieray, R. A., Whitten, W. B., and Ramsey, J. M.: The elucidation of Charge–Transfer–Induced Matrix effects in environmental aerosols via real-time aerosol mass spectral analysis of individual airborne particles, Aerosol Sci. Tech., 33, 135–152, 2000.

Reinard, M. S. and Johnston, M. V.: Ion formation mechanism in laser desorption ionization of individual nanoparticles, J. Am. Soc. Mass Spectr., 19, 389–399, 2008.

Robertson, J.: Diamond-like amorphous carbon, Mat. Sci. Eng., 37, 129–281, 2002.

Robinson, A. L., Donahue, N. M., Shrivastava, M. K., Weitkamp, E. A., Sage, A. M., Grieshop, A. P., Lane, T. E., Pierce, J. R., and Pandis, S. N.: Rethinking organic aerosols: Semivolatile emissions and photochemical aging, Science, 315, 1259–1262, 2007.

Saathoff, H., Naumann, K. H., Riemer, N., Kamm, S., Möhler, O., Schurath, U., Vogel, H., and Vogel, B.: The loss of NO_2, HNO_3, NO_3/N_2O_5, and $HO_2/HOONO_2$ on soot aerosol: a chamber and modeling study, Geophys. Res. Lett., 28, 1957–1960, 2001.

Saathoff, H., Moehler, O., Schurath, U., Kamm, S., Dippel, B., and Mihelcic, D.: The AIDA soot aerosol characterisation campaign 1999, J. Aerosol Sci., 34, 1277–1296, doi:10.1016/S0021-8502(03)00363-X, 2003.

Sandradewi, J., Prévôt, A. S., Szidat, S., Perron, N., Alfarra, M. R., Lanz, V. A., Weingartner, E., and Baltensperger, U.: Using aerosol light absorption measurements for the quantitative determination of wood burning and traffic emission contributions to particulate matter, Environ. Sci. Technol., 42, 3316–3323, 2008.

Scheier, P., Dünser, B., Wörgötter, R., Lezius, M., Robl, R., and Märk, T.: Appearance and ionization energies of singly, doubly and triply charged C_{60} and its fragment ions produced by electron impact ionization, Int. J. Mass Spectrom, 138, 77–93, 1994.

Schmid, J., Grob, B., Niessner, R., and Ivleva, N.: Multi-wavelength Raman microspectroscopy for rapid prediction of soot oxidation reactivity, Anal. Chem., 83, 1173–1179, doi:10.1021/ac102939w, 2011.

Schneider, J., Weimer, S., Drewnick, F., Borrmann, S., Helas, G., Gwaze, P., Schmid, O., Andreae, M., and Kirchner, U.: Mass spectrometric analysis and aerodynamic properties of various types of combustion-related aerosol particles, Int. J. Mass Spectrom., 258, 37–49, 2006.

Schwarz, J. P., Gao, R. S., Fahey, D. W., Thomson, D. S., Watts, L. A., Wilson, J. C., Reeves, J. M., Darbeheshti, M., Baumgardner, D. G., Kok, G. L., Chung, S. H., Schulz, M., Hendricks, J., Lauer, A., Kärcher, B., Slowik, J. G., Rosenlof, K. H., Thompson, T. L., Langford, A. O., Loewenstein, M., and Aikin, K. C.: Single-particle measurements of midlatitude black carbon and light-scattering aerosols from the boundary layer to the lower stratosphere, J. Geophys. Res., 111, D16207, doi:10.1029/2006JD007076, 2006.

Seinfeld, J. H. and Pandis, S. N.: Atmospheric chemistry and physics: from air pollution to climate change, John Wiley & Sons, New Jersey, USA, 2012.

Sellitti, C., Koenig, J., and Ishida, H.: Surface characterization of graphitized carbon fibers by attenuated total reflection Fourier transform infrared spectroscopy, Carbon, 28, 221–228, 1990.

Sevilla, M. and Fuertes, A. B.: Sustainable porous carbons with a superior performance for CO_2 capture, Energy Environ. Sci., 4, 1765–1771, 2011.

Shindell, D., Kuylenstierna, J., Vignati, E., van Dingenen, R., Amann, M., Klimont, Z., Anenberg, S., Muller, N., Janssens-Maenhout, G., Raes, F., Schwartz, J., Faluvegi, G., Pozzoli, L., Kupiainen, K., Höglund-Isaksson, L., Emberson, L., Streets, D., Ramanathan, V., Hicks, K., Oanh, N., Milly, G., Williams, M., Demkine, V., and Fowler, D.: Simultaneously mitigating near-term climate change and improving human health and food security, Science, 335, 183–189, doi:10.1126/science.1210026, 2012.

Slowik, J. G., Cross, E. S., Han, J.-H., Davidovits, P., Onasch, T. B., Jayne, J. T., Williams, L. R., Canagaratna, M. R., Worsnop, D. R., Chakrabarty, T. K., Moosmüller, J., Arnott, E. P., Schwarz, J. P., Gao, R.-S., Fahey, F. W., Kok, G. L., and Petzold, A.: An inter-comparison of instruments measuring black carbon content of soot particles, Aerosol Sci. Tech. 41, 295–314, doi:10.1080/02786820701197078, 2007.

Toner, S. M., Shields, L. G., Sodeman, D. A., and Prather, K. A.: Using mass spectral source signatures to apportion exhaust particles from gasoline and diesel powered vehicles in a freeway study using UF-ATOFMS, Atmos. Environ., 42, 568–581, 2008.

Tritscher, T., Jurányi, Z., Martin, M., Chirico, R., Gysel, M., Heringa, M. F., DeCarlo, P. F., Sierau, B., Prévôt, A. S., and Weingartner, E.: Changes of hygroscopicity and morphology during ageing of diesel soot, Environ. Res. Lett., 6, 034026, doi:10.1088/1748-9326/6/3/034026, 2011.

Vinke, P., Van der Eijk, M., Verbree, M., Voskamp, A., and Van Bekkum, H.: Modification of the surfaces of a gasactivated carbon and a chemically activated carbon with nitric acid, hypochlorite, and ammonia, Carbon, 32, 675–686, 1994.

von Helden, G., Hsu, M. T., Gotts, N., and Bowers, M. T.: Carbon cluster cations with up to 84 atoms: structures, formation mechanism, and reactivity, J. Phys. Chem., 97, 8182–8192, 1993.

Weingartner, E., Baltensperger, U., and Burtscher, H.: Growth and structural change of combustion aerosols at high relative humidity, Environ. Sci. Technol., 29, 2982–2986, 1995.

Wiedensohler, A., Birmili, W., Nowak, A., Sonntag, A., Weinhold, K., Merkel, M., Wehner, B., Tuch, T., Pfeifer, S., Fiebig, M., Fjäraa, A. M., Asmi, E., Sellegri, K., Depuy, R., Venzac, H., Villani, P., Laj, P., Aalto, P., Ogren, J. A., Swietlicki, E., Williams, P., Roldin, P., Quincey, P., Hüglin, C., Fierz-Schmidhauser, R., Gysel, M., Weingartner, E., Riccobono, F., Santos, S., Grüning, C., Faloon, K., Beddows, D., Harrison, R., Monahan, C., Jennings, S. G., O'Dowd, C. D., Marinoni, A., Horn, H.-G., Keck, L., Jiang, J., Scheckman, J., McMurry, P. H., Deng, Z., Zhao, C. S., Moerman, M., Henzing, B., de Leeuw, G., Löschau, G., and Bastian, S.: Mobility particle size spectrometers: harmonization of technical standards and data structure to facilitate high quality long-term observations of atmospheric particle number size distributions, Atmos. Meas. Tech., 5, 657–685, doi:10.5194/amt-5-657-2012, 2012.

Winklmayr, W., Reischl, G. P., Lindner, A. O., and Berner, A.: A new electromobility spectrometer for the measurement of aerosol size distributions in the size range from 1 to 1000 nm, J. Aerosol Sci., 22, 289–296, 1991.

Zencak, Z., Elmquist, M., and Gustafsson, Ö.: Quantification and radiocarbon source apportionment of black carbon in atmospheric aerosols using the CTO-375 method, Atmos. Environ., 41, 7895–7906, 2007.

Zhang, Q., Jimenez, J. L., Canagaratna, M. R., Ulbrich, I. M., Ng, N. L., Worsnop, D. R., and Sun, Y.: Understanding atmospheric organic aerosols via factor analysis of aerosol mass spectrometry: a review, Anal. Bioanal. Chem., 401, 3045–3067, 2011.

Zielke, U., Hüttinger, K., and Hoffman, W.: Surface-oxidized carbon fibers: I. Surface structure and chemistry, Carbon, 34, 983–998, 1996.

Zimmerman, J. A., Eyler, J. R., Bach, S. B., and McElvany, S. W.: "Magic number" carbon clusters: ionization potentials and selective reactivity, J. Chem. Phys., 94, 3556–3562, 1991.